https://doi.org/10.1595/205651321X16038755164270 *Johnson Matthey Technol. Rev.*, 2021, **65**, (4), 556–567

JOHNSON MATTHEY
TECHNOLOGY REVIEW
www.technology.matthey.com

Study of Ultrasonic Attenuation and Thermal Conduction in Bimetallic Gold/Platinum Nanofluids

Effect of thermal conductivity on ultrasonic attenuation of gold and gold/platinum nanofluids

Alok Kumar Verma
Department of Physics, Prof. Rajendra Singh (Rajju Bhaiya) Institute of Physical Sciences for Study and Research, Veer Bahadur Singh Purvanchal University, Jaunpur-222003, Uttar Pradesh, India

Navneet Yadav*
Department of Physics, University of Allahabad, Allahabad-211002, India

Shakti Pratap Singh
Department of Physics, Prof. Rajendra Singh (Rajju Bhaiya) Institute of Physical Sciences for Study and Research, Veer Bahadur Singh Purvanchal University, Jaunpur-222003, Uttar Pradesh, India

Kajal Kumar Dey
Centre for Nanoscience and Technology, Prof. Rajendra Singh (Rajju Bhaiya) Institute of Physical Sciences for Study and Research, Veer Bahadur Singh Purvanchal University, Jaunpur-222003, Uttar Pradesh, India

Devraj Singh
Department of Physics, Prof. Rajendra Singh (Rajju Bhaiya) Institute of Physical Sciences for Study and Research, Veer Bahadur Singh Purvanchal University, Jaunpur-222003, Uttar Pradesh, India

Raja Ram Yadav
Department of Physics, Prof. Rajendra Singh (Rajju Bhaiya) Institute of Physical Sciences for Study and Research, Veer Bahadur Singh Purvanchal University, Jaunpur-222003, Uttar Pradesh, India; Department of Physics, University of Allahabad, Allahabad-211002, India

***Email:** navneetyadav@allduniv.ac.in

Here, we report the frequency dependent ultrasonic attenuation of monometallic gold and bimetallic gold/platinum based aqueous nanofluids (NFs). The as-synthesised bimetallic NFs (BMNFs) revealed less resistance to ultrasonic waves compared to the monometallic NFs. Thermal conductivity of both NFs taken at different concentrations revealed substantial conductivity improvement when compared to the base fluid, although gold/platinum showed lesser improvement compared to gold. Characterisation of the as-synthesised nanoparticles (NPs) and fluids was carried out with X-ray diffraction (XRD), ultraviolet-visible (UV-vis) spectroscopy, transmission electron microscopy (TEM) and energy-dispersive X-ray spectroscopy (EDS). The distinct two-phase bimetallic nature of gold/platinum, its two plasmonic band optical absorption features and the spherical morphology of the particles were shown. The findings were correlated with the observed thermal and ultrasonic behaviour and proper rationalisation is provided. It

was revealed that the comparatively lesser thermal conductivity of gold/platinum had direct implication on its attenuation property. The findings could have important repercussions in both industrial applications and in the mechanistic approach towards the field of ultrasonic attenuation in NFs.

1. Introduction

Synthesis and analysis of metallic NPs having different configurations, properties, morphologies and sizes has attracted extensive interest in the research community (1–3). In recent years, much attention has been paid to the fabrication of colloidal bimetallic NPs (BMNPs) due to their superior catalytic, electric, magnetic and optical properties over monometallic NPs and a wide range of applications in sensors, catalysis, biomedical imaging, optochemical sensors, drug delivery systems and quantum dots (4–8). Incorporation of a second metal not only modifies physicochemical characteristics of their constituent parts but also offers novel characteristics because of synergistic interactions between the components (9). As a case in point, Singh *et al*. (10) studied the catalytic activity of bimetallic nickel-palladium NPs ($Ni_{0.60}Pd_{0.40}$) and found a high hydrogen selectivity (>80%) for the decomposition of hydrous hydrazine at 323 K. The corresponding monometallic counterparts were either poorly active (nickel NPs) or inactive (palladium NPs). Feng *et al*. (11) observed significantly higher catalytic activity for the bimetallic gold/platinum nanodendrites towards oxidation of methanol when compared to the commercial platinum/carbon catalyst. They rationalised this result through enhanced electronic interaction among its constituents. Toupkanloo *et al*. (12) synthesised palladium/silver BMNPs by a conventional reduction method aided by sound waves and reported increased viscosity for ethylene glycol with the incorporation of the palladium/silver BMNPs. They also reported quite significant enhancement in the electrical conductivity of aqueous medium when incorporated with the above BMNPs and compared the data favourably with monometallic counterparts. Kumari *et al*. (13) fabricated gold/silver BMNFs using the juice of pomegranate fruit and reported enhanced catalytic activity and nitric oxide and hydroxyl radical scavenging activity by the bimetallic species. The enhanced properties of BMNPs make them good candidates for various industrial, research and medical applications. Thus, BMNPs have become a hot topic for researchers and scientists across various interests.

Among the various bimetallic combinations being explored by contemporary researchers, the pairing of gold and platinum NPs appears very frequently. Gold NPs have a wide array of applications as a direct consequence of having a wide absorption band over the visible region in fields such as: molecular imaging in plasmonic photothermal therapy; organic photovoltaics; as a therapeutic agent in biomedical application; as sensory probes and in electronic conductors (14–16). An extremely important feature of gold NPs is the tunable optoelectronic property which can be tailored based on the size, morphology and aggregation rate of the particles (17, 18). Platinum NPs, on the other hand, have superior antioxidation and catalytic properties used in petrochemical cracking and electrocatalysis (19, 20). As a functional metal, platinum NPs, owing to their suitable Fermi level positioning and excellent electron interaction kinetics, can be utilised in hydrogen evolution and oxygen reduction reactions as an electrocatalyst (21). However, bimetallic gold/platinum NPs have shown impressive and in most instances superior performances in various applications compared to either of its constituents: gold and platinum (22–26).

Efforts have been devoted towards obtaining gold/platinum BMNPs with excellent optical, electronic and surface properties. For example, Bian *et al*. reported the synthesis of twinned gold-platinum core-shell star-shaped decahedra through epitaxial growth (23). Bao *et al*. reported the preparation of gold-platinum core–shell nanorods for *in situ* examination of catalytic reactions employing surface enhanced Raman scattering spectroscopy (24). Fang *et al*. reported the formation of gold/platinum hollow bypyramid frames by a simple mixing of the respective precursors (25). They reported that this configuration allows the excellent plasmonic property of the gold NPs to couple with the highly active catalytic sites of platinum, making it the ideal multifunctional platform for catalysing and monitoring reactions in real time. Yu and his group reported the fabrication of gold-platinum bimetallic alloy on palladium nanocubes for hydrogen peroxide oxidation (26). Their motivation was to balance the low hydrogen conversion of gold with the high hydrogen conversion ability of platinum and the low selectivity of platinum with the high selectivity of gold. They reported a much better hydrogen peroxide production for the bimetallic catalyst as a result of the carefully choreographed synergistic effects of gold and platinum. The growth of platinum NPs on gold nanoplates with excellent photoresponse has also been reported. Lou *et al*. reported the fabrication of anisotropic

platinum loaded triangular gold nanoprisms as photocatalysts for hydrogen generation reaction (27). Zhang and Toshima have reported a simultaneous reduction method to prepare gold/platinum BMNPs for superior and stable catalytic activity in aerobic glucose oxidation (28). As gold-platinum BMNPs show a third order nonlinear phenomenon due to strong optical Kerr effect, it can be an excellent contender for the development of low dimensional gyroscopic systems (29).

Acoustic attenuation spectroscopy is a relatively new technique to characterise the stability and structure of semisolid topical delivery systems for cosmetic and pharmaceutical applications (30). Ultrasonic attenuation techniques have provided a new dimension to non-destructive testing (NDT) of highly sophisticated materials. It provides the particle size distribution (PSD) of suspended solid particles in a highly precise manner. Ultrasonic NDT offers material characterisation not only after fabrication but also during the processing of materials (31). High energy acoustic waves have been extensively used in both the industrial sector as well as in medical sciences. Controlling material characteristics by monitoring physical parameters such as structural inhomogeneity, elastic constants, thermal conductivity, phase transformation, size and dislocation that forecast potential use of the materials can be accomplished by determining frequency dependent ultrasonic absorption. Acoustic attenuation may also be utilised for extensional rheology determination (32, 33).

The past few decades have witnessed several research groups investigating the ultrasonic behaviour of aqueous solutions in search of a comprehensive mechanism so that better control over the procedure could be achieved (34–36). For fluidic suspensions, it has been found that in general microsized dispersants tend to lessen the wave propagation due to weak particle-liquid interaction whereas nanosized particles enhance the wave propagation due to increased particle-liquid interaction (34). NPs in fluids (known as NFs) present a fascinating case study for understanding the physical mechanisms governing the ultrasonic behaviour in liquid suspensions because of the wide varieties of manipulations that can be achieved by changing their compositions, concentrations or chemical nature. A decreased attenuation in NFs could lead to a better performance in ultrasound imaging techniques. Attenuation also affects the propagation of waves and signals in electrical circuits, optical fibres and in air, making this phenomenon a critical one in the fields of electrical engineering and telecommunications. It is thus imperative to develop fluidic systems with enhanced wave propagation or decreased attenuation properties that can account for a better performance in the above areas. Aqueous metallic NFs which are already heavily sought after due to their interesting plasmonic properties (30) could add value with impressive ultrasound properties. So far, only a handful of studies have been conducted on the ultrasonic properties of metallic NFs (30, 34). The combined study of ultrasonic and thermal properties and in particular effect of ultrasonic wave propagation on the thermal conductivity or *vice versa* for metallic NFs is, to the best of our knowledge, yet to be reported.

In this article we report the attenuation properties of gold monometallic and gold/platinum BMNFs. We observed that the attenuation property was lower in the BMNF compared to the monometallic one. We have also observed the thermal conductivity properties of both the NFs and have been able to rationalise our observation based on the physiochemical data at our disposal. A simple correlation between our observed attenuation and thermal conductivity properties combined with theoretical background provides us with the physical explanation for the decreased attenuation properties in the BMNF.

2. Materials and Methods

The precursors used in the synthesis of BMNFs were hydrogen tetrachloroaurate(III) trihydrate ($HAuCl_4 \cdot 3H_2O$) and hexachloroplatinic(IV) acid hydrate ($H_2PtCl_6 \cdot xH_2O$) obtained from HiMedia Laboratories Pvt Ltd, India. Trisodium citrate ($Na_3C_6H_5O_7$) was purchased from Merck KGaA, Germany. The chemicals used were reagent grade and were used without further purification. The synthesis of the metallic NFs were conducted following previously reported procedure (37). Briefly, 0.1 wt% solution of $HAuCl_4 \cdot 3H_2O$ (10 ml) was stirred robustly and boiled. An aqueous solution of 1.0 wt% of $Na_3C_6H_5O_7$ (2 ml) was mixed in the above solution in a dropwise manner and was subsequently stirred for 5 min. The colour transformation from light yellow to vivid magenta after the addition of $Na_3C_6H_5O_7$ indicates the development of stable gold NF. For the preparation of BMNFs, 10 ml 0.1 wt% aqueous solution of H_2PtCl_6 was added to this NF followed by the further addition of 2 ml 1.0 wt% aqueous solution of $Na_3C_6H_5O_7$ with concomitant vigorous stirring; the entire solution being kept at room temperature. The final solution was heated

up in a microwave oven in a cyclical on/off manner for 5 min (on 15 s, off 5 s). The cyclical process was accommodated to avoid extreme boiling and aggregation of the reaction components. The solution turned to greyish following the microwave treatment indicating the formation of gold/platinum BMNFs (35). The flowchart for the synthesis process of gold/platinum BMNFs has been presented in **Figure 1**.

The crystalline nature and phases of gold/platinum BMNPs were examined by X'Pert PRO diffractometer (PANalytical, The Netherlands) having monochromatic Cu-Kα radiation (λ = 1.5406 Å). NFs were drop cast on a cleaned glass substrate and the as-deposited thin films were utilised for the XRD technique. EDS and elemental analysis of gold NFs and gold/platinum BMNFs were done by the TEAM™ EDS analysis system with Octane Plus silicon drift detector (SDD) (EDAX Inc, USA). Microstructural morphology and reciprocal space analysis of the synthesised materials were conducted by the high-resolution TEM (HRTEM; Tecnai™ G^2 F30 S-TWIN, FEI Company, USA). Optical properties were evaluated using a LAMBDA™ 35 UV-vis spectrophotometer (PerkinElmer Inc, USA). PSD and frequency and concentration dependent ultrasonic attenuation at room temperature in both the NFs were determined by APS-100 acoustical particle sizer (Matec Applied Sciences, USA).

Thermal conductivities of gold NFs and gold/platinum BMNFs were determined by the Hot Disk TPS 500 Thermal Constants Analyser (Hot Disk AB, Sweden) which works on the principle of transient plane source (TPS) method. The TPS technique is the advanced version of transient hot wire (THW) technique. In this technique, Fourier's law of heat conduction is used to measure the value of thermal conductivity of the subject materials. The technique corresponds to uncertainties of about 2%.

3. Results and Discussion

3.1 Structural Analysis, EDS Spectra and Elemental Mapping

Figure 2 shows the XRD pattern of bimetallic gold/platinum NFs. The pattern does not indicate gold-platinum alloy configurations but confirms the two phases: gold and platinum of the BMNPs individually. This may be due to the thermal immiscibility of gold and platinum at low temperature. The pattern shows diffraction peaks at 2θ = 38.52º, 44.23º, 64.06º and 77.68º corresponding to (*hkl*) planes (111), (200), (220) and (311) respectively of the face centred cubic (fcc) gold structure having a lattice constant of 4.078 Å (Joint Committee on Powder Diffraction Standards (JCPDS) No. 04-0784). Additional and relatively diminutive peaks obtained

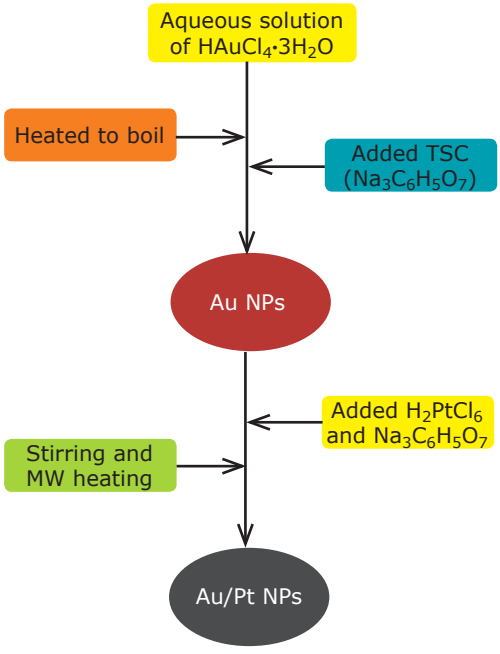

Fig. 1. Flow chart for synthesis of gold/platinum BMNFs

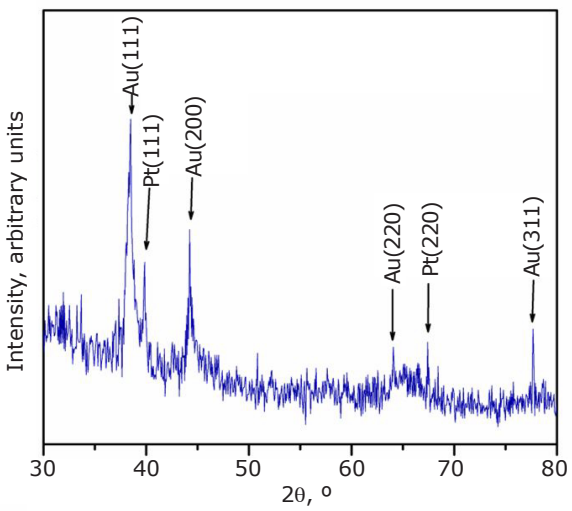

Fig. 2. XRD pattern of gold/platinum BMNFs

at 2θ = 39.72º and 67.47º correspond respectively to the (*hkl*) planes (111) and (220) of the fcc crystal structure of platinum with a lattice constant of 3.923Å (JCPDS No. 04-0802). The average crystallite sizes (D) of the two phases of BMNPs have been calculated using the Scherrer equation (Equation (i)) (38):

$$D = 0.9\lambda/\beta\cos\theta \quad \text{(i)}$$

where β is full width at half maxima (FWHM) in radian, θ is the position of the peak in degrees, and λ is the wavelength of X-ray. The average crystallite size for gold NPs and platinum NPs were calculated to be 19.4 nm and 31.3 nm respectively. This mathematical inference tallies well with the visual intuition obtained from the relatively wider diffraction peak of the gold NPs (**Figure 2**).

The elemental composition of the as-synthesised materials has been examined *via* EDS method (**Figure 3**). From the corresponding spectrum both gold and platinum were detected confirming the bimetallic nature of the sample. The atomic percentage was estimated to be Au:Pt = 71.28:21.72. Some extra peaks were also observed in the EDS spectrum corresponding to carbon and copper; the origin of which can be attributed to the carbon coated copper grid upon which the NFs were deposited for the EDS analysis. So, while calculating the atomic percentages these were ignored. The elemental mappings of the gold/platinum BMNFs are shown by **Figure 4**. **Figures 4(a)** and **4(b)** show the independent distribution of gold and platinum NPs respectively while **Figure 4(c)** reveals the distribution of gold and platinum taken together in gold/platinum BMNFs. As was observed from the images, both the metallic particles were homogeneously distributed within the experimental range; however, the

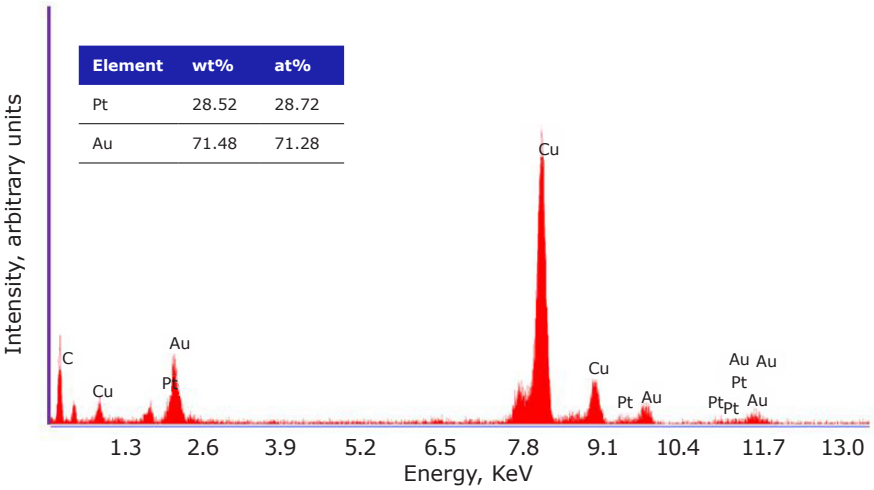

Fig. 3. EDS pattern spectra of gold/platinum BMNFs. Inset table shows weight and atomic percentage of gold and platinum elements

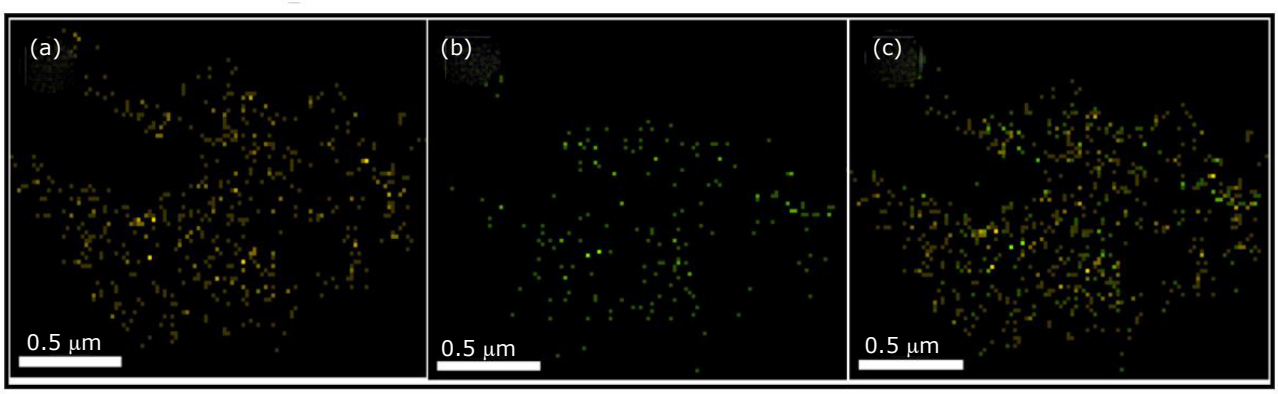

Fig. 4. Elemental mappings of: (a) gold; (b) platinum; (c) gold/platinum BMNFs

concentration of gold NPs was clearly denser as compared to the platinum NPs, an observation that vindicates the findings of the EDS spectrum.

3.2 Particle Size Distribution and Microstructural Analysis

Microstructural analysis and the size distribution of the as-synthesised BMNF were carried out through TEM images. **Figure 5(a)** provides a collection of closely spaced gold/platinum bimetallic NPs. A more magnified view of the image reveals the almost spherical nature of the particles (**Figure 5(b)**). The distortion in the spherical morphology is slight and sometimes leads to the appearance of semi-ellipsoidal particle shape. Particle sizes estimated from a large group of particles such as observed in **Figure 5(a)** indicated that almost all the particles conform to such spherical/spheroidal morphology with average particle size staying within the range of 15–30 nm. **Figure 5(c)** displays the high resolution TEM micrograph of a single particle. Clear visible lattice fringes were indexed and the lattice planes matched well with the gold (200; *d* spacing = 0.204 nm, JCPDS - 04-0784) and platinum (111; *d* spacing = 0.231 nm, JCPDS - 04-0802) fcc crystal, indicating the simultaneous presence of gold and platinum lattice within the particle and confirming its bimetallic nature. The selected area electron diffraction (SAED) pattern is used to describe crystallinity of the NPs and is shown in the **Figure 5(d)**. The unblemished ring pattern observed indicates the polycrystalline nature of the bimetallic particles which is well in agreement with observations from the XRD patterns (**Figure 2**).

PSD of NPs in both gold monometallic and gold/platinum BMNFs was studied by APS-100 acoustic particle sizer. This analysis method provides a PSD without any prior knowledge of the shape of the particles or even if the solution is concentrated. The APS-100 obtains the PSD data from the acoustic attenuation spectroscopy measurements. Usually as sound travels through a colloidal medium, it gets attenuated and this level of attenuation is related to the corresponding particle size within the colloidal solution. The as-obtained normalised PSD curves for both the monometallic gold and bimetallic gold/platinum NFs are displayed in **Figure 6**. An interesting observation here is that particles in BMNFs are slightly larger in size compared to that of monometallic NFs. The reason for this may be the larger crystallite sizes of platinum zones as observed from the XRD pattern, leading to an enhancement of the particle sizes when the platinum crystallites are incorporated. The size distribution of NPs in gold/platinum BMNFs is wider when compared to that of the monometallic gold NFs. Overall, the size of the dispersed NPs was found to be in the range of 19 nm to 30 nm

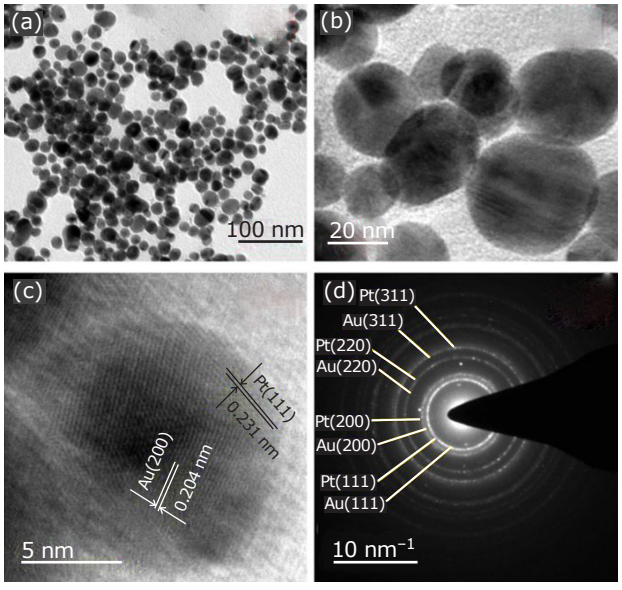

Fig. 5. (a)–(c) HRTEM images of gold/platinum BMNFs; (d) corresponding SAED pattern

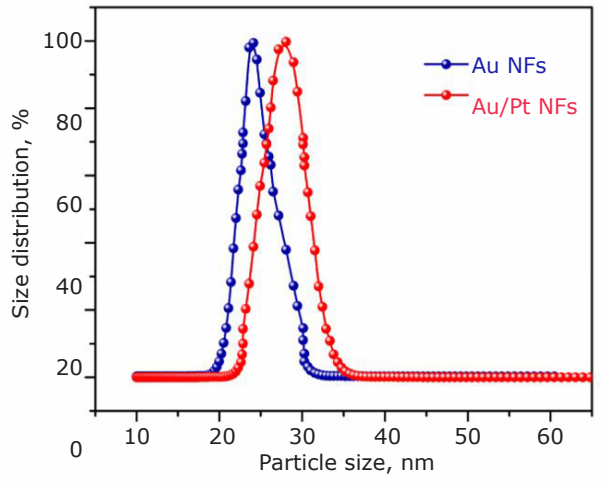

Fig. 6. PSD of gold monometallic NFs and gold/platinum BMNFs by APS-100

for the gold NFs and 22 nm to 36 nm for the gold/platinum BMNFs. The maximum distribution is found at ~23 nm for the monometallic and at ~27 nm for the bimetallic NPs. The obtained particle size range is slightly larger from that observed in the TEM micrograph (**Figure 5**), which could be due to the localised nature of TEM analysis or simply because of the variation observed as a consequence of the difference between a direct optical method and an indirect acoustic method of determination.

3.3 Optical Characteristics and Surface Plasmon Resonance Band Nature

UV-vis absorption spectroscopy was carried out to analyse the band structure of the metallic samples and to further confirm the formation of the gold monometallic and the gold/platinum bimetallic NPs. **Figure 7** shows the absorption spectra of the bimetallic gold/platinum and monometallic gold NFs. Gold NPs of spherical nature usually display surface plasmon resonance (SPR) absorption band at ~520 nm which can be shifted depending on the size, shape and environment of the particles (39, 40). The absorption peak of gold NF was obtained at 529 nm and the slight red shift could have been a result of the less than perfect spherical shape of the particles as observed from the TEM micrographs (**Figure 5**). The absorption peak of the gold/platinum BMNF is obtained at 542 nm indicating the dominance of gold NP in the overall absorbance feature of the bimetallic species. It also confirms the surface disposition of the gold NPs alongside platinum. Otherwise, platinum would have overwhelmed the SPR characteristics of gold and a featureless absorbance spectrum could have been obtained, as is usually observed for platinum in the visible region. The reason for apparent red shift (529 nm → 542 nm) could be an increased asymmetry in the shape of the gold NPs. But since the gold has been synthesised beforehand, that scenario should be ignored, as platinum particles affecting the shape of the gold NPs is pretty unlikely. No alloying was detected in the XRD pattern of the particles and so shifting due to alloying is also unlikely. So, the only possible reason for the shifting could be the change of the dielectric environment of the gold NPs due to the presence of platinum around them. The other broad absorption peak observed at 634 nm for the bimetallic gold/platinum NF could be attributed to the relative aggregation of gold NPs due to slight decrease in its surface charge as a result of platinum incorporation. The aggregation would lead to dielectric coupling between the particles leading to a broad absorption band north of 600 nm (41). The shifting in the SPR band in the visible region indicates the possible use of the BMNFs in the fabrication of optochemical sensors and as an effective photocatalyst (42, 43).

3.4 Ultrasonic Attenuation and Thermal Conductivity

Frequency and concentration dependent ultrasonic attenuation were measured in monometallic and BMNFs at room temperature and the obtained

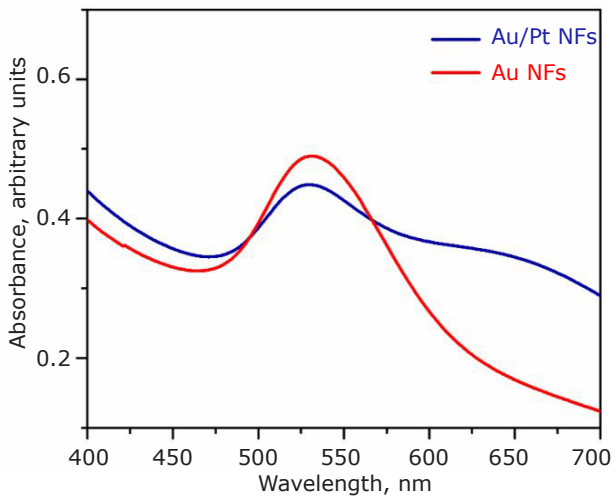

Fig. 7. UV-vis spectra of gold and gold/platinum BMNF

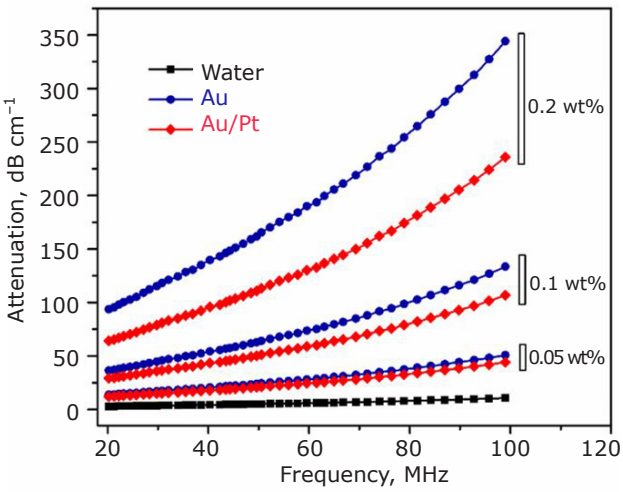

Fig. 8. Ultrasonic attenuations in gold monometallic NFs and gold/platinum BMNFs at different concentrations

results are provided in **Figure 8**. Evidently, the attenuation in both the NFs increases with increasing frequency. The increment is almost linear up to a certain frequency range beyond which it accelerates faster and the relationship apparently becomes non-linear. Sound waves become more attenuated in the NFs as compared to pure water. Furthermore, it is clear that attenuation is lower in the BMNFs than monometallic gold NFs.

Ultrasonic attenuation is highly sensitive to the local environment of the medium (44–46). Here, the macroscopic interfaces of mono and bimetallic NPs with water molecules become a vital factor to regulate their final values. The effective sound absorption by NPs in base matrix suspensions may be stated as Equation (ii):

$$\alpha = \alpha_m + \alpha_b + \alpha_{mb} \quad \text{(ii)}$$

where α_m is the attenuation due to metal NPs, α_b is the corresponding part of absorption due to the base matrix and α_{mb} is the modification to the final value of α due to the interaction between metal NPs and base-fluids molecules in conjunction with modified thermomechanical characteristics of nanocolloidal suspensions (47).

The characteristic absorption of the sound wave due to individual particles is usually insignificant (48, 49). Existence of a stable interface between NP and base matrix molecules plays a significant role in determining the value of α_{mb}. Factors affecting attenuation properties for different particle-fluid combinations have been explored previously. Kor *et al.* (50) investigated ultrasonic attenuation in gold due to phonon-phonon interaction, electron phonon interaction and thermoelastic loss. They reported total ultrasonic attenuation ~3 dB cm^{-1} along <100> direction and ~6 dB cm^{-1} along <110> direction. So, the nature of the facets plays an important role in determining the extent of attenuation. In general, the total sound attenuation in the NP-liquid suspensions depends upon scattering loss, viscous loss and thermal loss (51, 52). Biwa *et al*. (53) investigated the sound attenuation in liquid suspensions having millimetre sized particles using a differential scheme. They reported significant particle-reinforced attenuation due to scattering of the wave. But in case of colloidal dispersions or for nanosized particles, the particle sizes are usually smaller than the sound wavelength and as a result dissipative process rather than the scattering process govern the acoustical behaviour of such systems (54). So, for the time being it may be assumed that viscous loss and thermal loss are to play major roles in determining the acoustical properties of the present NF systems.

The expressions for thermal wavelength (Λ_T) and viscous wavelength (Λ_V) (Equations (iii) and (iv)) (55):

$$\Lambda_T = \sqrt{2K/(\rho C\omega)} \quad \text{(iii)}$$

where K, ρ and C are thermal conductivity, density and specific heat of the suspended particles and ω is the frequency of the sound wave.

$$\Lambda_V = \sqrt{2\eta/(\sigma\omega)} \quad \text{(iv)}$$

where η is the viscosity of the base fluid.

In the present case, calculated values of Λ_T and Λ_V are of the order of 10^{-6} m and 10^{-7} m respectively for 10 MHz frequency which is not comparable to the size of the suspended metallic NPs. Thus, attenuation due to the viscous loss and thermal loss can be treated as insignificant. So, the behaviour of the whole curve can be explained in terms of effective attenuation due to interaction between acoustic phonon and lattice phonon of dispersed crystal in conjunction with Brownian motion induced enhanced thermal conductivity (K) of the NFs. The calculated value of thermal relaxation time for gold crystal is of the order of 10^{-10} s (50). The condition $\omega t \ll 1$ is maintained for the frequency range of 10 MHz to 100 MHz for the determination of effective attenuation which is directly proportional to thermal relaxation time (τ) Equation (v):

$$\tau = 3\,K/(C_V(\overline{V}^2)) \quad \text{(v)}$$

where C_V denotes specific heat per unit volume and $\overline{V}$ denotes Debye average velocity. Thus, it may be assumed that the attenuation in the NFs is directly proportional to their individual thermal conductivity.

These results of the gold/platinum BMNFs may be confronted with recent developments in the field of ultrasonic studies of similar type of BMNFs. Hurtado-Aviles *et al.* (29) observed strong influence of ultrasonic waves on the optical and plasmonic properties of ethanol-based gold-platinum BMNFs which is very effective for instrumentation and low-dimensional signal processing.

Figure 9 displays concentration dependent thermal conductivity of the monometallic and BMNFs at room temperature. It indicates that thermal conductivity of both the NFs increases with NPs loading. Another notable observation is that the conductivity is consistently lower in the bimetallic species as compared to the monometallic species. At room temperature (27ºC) and at 0.05 wt% concentration the thermal conductivity of the

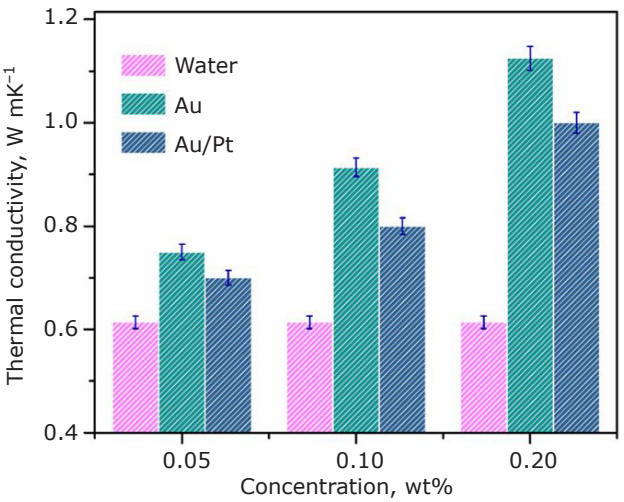

Fig. 9. Thermal conductivity of gold monometallic NFs and gold/platinum BMNFs

gold NF and the gold/platinum BMNF was found to be 0.75 W mK^{-1} and 0.7 W mK^{-1} respectively or having a ratio of K_{bi}:K_{mono} = 0.93. At 0.2 wt% the thermal conductivity of gold NFs and gold/platinum BMNFs were estimated to 1.12 W mK^{-1} and 0.99 W mK^{-1} respectively i.e., having a ratio of 0.88. So, with increasing concentration the thermal conductivity of the monometallic NF enhances at a slightly faster rate compared to that of the gold/platinum BMNFs. So, the present observation of the ultrasonic attenuation being lower in the BMNF can be rationalised from the comparative thermal conductivity behaviour of the two NFs.

There is no specific model for explaining the thermal conductivity behaviour of BMNFs. Most of the traditionally utilised models for composite materials such as Maxwell-Garnett do not properly explain the enhancement in NFs where nanosized particles have direct interfacial interactions with the matrix; fluid in this case (56). A subsequent model proposed by Kumar *et al*. (57) was somewhat appropriate in rationalising the thermal conductivity behaviour of the NFs. They incorporated the idea of parallel thermal conductivity between the NPs and the liquid particles. They explained the variation of thermal conductivity in the NF with temperature as being due to the variation in particle velocity with temperature. Subsequent researchers have proposed that the Brownian motion of the particles intensifies in the NF with increased temperature and volume fraction of the NPs in base fluid, while its effects diminish with increasing particle size (57, 58). Kumar *et al*. in their paper also countered the argument of interfacial resistance in such systems by proposing that the surface interaction is facilitated by the larger specific surface area of the nanosized particles (57). According to their proposed model, the expression for thermal conductivity of NP-liquid suspensions could be explained by Equation (vi):

$$k = k_f \left[1 + \frac{\phi\, k_n r_f}{k_f (1 - \phi) r_n} \right] \qquad \text{(vi)}$$

where k is thermal conductivity of the NF and the subscripts f and n represent base fluid and NP respectively. It is obvious from the above equation, that thermal conductivity enhancement is linearly proportional to concentration of NPs (Φ) and inversely proportional to the radius (r) of the NPs. Significant enhancement in thermal conductivity at small concentration of the suspended NPs can be described using this model.

Past research on gold/platinum systems has shown that the thermal conductivity of the solid system depends on its composition (59). Metallic gold has significantly higher thermal conductivity compared to metallic platinum. At a lower percentage of gold, the system could potentially be occupied by individual single metallic phases and understandably, the thermal conductivity of that system, being an average of its components, would be lower as compared to pure gold solid system. Prior literature reveals that gold/platinum system could potentially start to form an alloy at the composition of about 70 at% gold, following which the thermal conductivity of the solid system could rise again (59). But the thermal conductivity of the system always stays well below that of single-phase gold. This would explain why the present gold/platinum nanoparticulate system would have a thermal conductivity lower than the gold NP system and in turn, as per Equation (vi), would explain the lower thermal conductivity of the BMNF system compared to the gold monometallic system. Additionally, as observed from the APS-100 measurements, the average particle sizes of gold NPs are slightly lower than that of the average particle sizes of platinum. The smaller particle size of gold could mean a higher thermal conductivity and consequently a higher enhancement of thermal conductivity for the gold NF compared to the gold/platinum BMNF. Of course, as mentioned before, the exact mechanisms for the thermal conductivity within a NF is still not understood. It could be either of the above factors individually or a combination between the two that results in the lower thermal conductivity of the bimetallic moiety.

Thus, the reduced thermal conductivity in gold/platinum NFs in turn reduces sound attenuation

in gold/platinum NFs. As already explained, the attenuation property can be directly proportional to the NFs thermal conductivity, thus a reduction in the NF thermal conductivity results in loss of attenuation capability. The above results of ultrasonic studies of gold/platinum BMNFs should prove to be of significant implications in various industrial applications such as ultrasound imaging, extensional rheology, optochemical sensors, petrochemical cracking and therapeutic agents in the biomedical field.

4. Conclusions

Gold monometallic and gold/platinum BMNFs were synthesised *via* a simple microwave induced citrate reduction. The NFs were characterised in detail *via* various methods such as XRD which revealed a distinct two-phase bimetallic crystal structure without any alloy formation and by UV-vis which revealed the presence of two plasmonic bands in the bimetallic species with a tendency for aggregation. The elemental analysis further confirmed a bimetallic nature of the gold/platinum NFs. High resolution microscopy study revealed spherical NPs within the size range of 15–30 nm with well delineated lattice spacings belonging to both gold and platinum. The APS-100 studies revealed that the bimetallic NPs were of slightly larger particle size when compared to the monometallic ones. The ultrasonic characteristics of both the NFs were studied in conjunction with their thermal behaviour. The attenuation studies revealed that the BMNF has reduced attenuation when compared to the monometallic NF. The thermal studies conducted revealed that both the NFs had enhanced thermal conductivity compared to the base fluid which in this case was water. The gold/platinum NF was revealed to have slightly lower thermal conductivity compared to gold, which could be explained by its mixed metallic structure where platinum with a much lower thermal conductivity reduces the overall thermal conductivity of the bimetallic species. The lower thermal conductivity could perfectly explain the lower attenuation of the BMNF as previous studies had revealed that thermal conductivity is proportional to ultrasonic attenuation. The finding that gold/platinum BMNF could have lower attenuation as a result of lower thermal conductivity compared to monometallic gold NF can have significant repercussions in varied fields such as ultrasound imaging, extensional rheology and optochemical sensors.

Acknowledgments

Navneet Yadav acknowledges the financial support provided by the University Grants Commission, India.

References

1. M. Dao, L. Lu, R. J. Asaro, J. T. M. De Hosson and E. Ma, *Acta Mater.*, 2007, **55**, (12), 4041
2. I. De la Calle, M. Menta and F. Séby, *Spectrochim. Acta B: Atom. Spectrosc.*, 2016, **125**, 66
3. X. Feng, C. Wang, H. Ma, Y. Chen, G. Duan, P. Zhang and G. Song, *Mod. Phys. Lett. B*, 2018, **32**, (04), 1850046
4. N. R. N. Roselina, A. Azizan, K. M. Hyie, M. C. Murad and A. H. Abdullah, *Int. J. Mod. Phys. B*, 2015, **29**, (10n11), 1540006
5. A. Zaleska-Medynska, M. Marchelek, M. Diak and E. Grabowska, *Adv. Colloid Interface Sci.*, 2016, **229**, 80
6. H.-J. Chen, Y.-H. Wang, Y.-X. Zhang, X.-J. Zhang, C.-P. Jiao and H.-J. Zhang, *Mater. Res. Innov.*, 2017, **22**, (5), 267
7. H. Zhang and N. Toshima, *Appl. Catal. A: Gen.*, 2012, **447**–**448**, 81
8. H. Peng, W. Qi, W. Ji, S. Li and J. He, *Int. J. Mod. Phys. B*, 2017, **31**, (07), 1741012
9. D. Kim, J. Resasco, Y. Yu, A. M. Asiri and P. Yang, *Nat. Commun.*, 2014, **5**, 4948
10. S. K. Singh, Y. Iizuka and Q. Xu, *Int. J. Hydrogen Energy*, 2011, **36**, (18), 11794
11. Y. Feng, H. Liu and J. Yang, *J. Mater. Chem. A*, 2014, **2**, (17), 6130
12. H. Azizi-Toupkanloo, E. K. Goharshadi and P. Nancarrow, *Adv. Powder Technol.*, 2014, **25**, (2), 801
13. M. M. Kumari, J. Jacob and D. Philip, *Spectrochim. Acta A: Mol. Biomol. Spectrosc.*, 2015, **137**, 185
14. R. Popovtzer, A. Agrawal, N. A. Kotov, A. Popovtzer, J. Balter, T. E. Carey and R. Kopelman, *Nano Lett.*, 2008, **8**, (12), 4593
15. X. Huang and M. A. El-Sayed, *Alexandria J. Med.*, 2011, **47**, (1), 1
16. G. Chirico, M. Borzenkov and P. Pallavicini, "Gold Nanostars: Synthesis, Properties and Biomedical Application", Springer International Publishing, Cham, Switzerland, 2015, 80 pp
17. M.-C. Daniel and D. Astruc, *Chem. Rev.*, 2004, **104**, (1), 293
18. J.-H. Lee, S. U. S. Choi, S. P. Jang and S. Y. Lee, *Nanoscale Res. Lett.*, 2012, **7**, 420
19. J. Kim, M. Takahashi, T. Shimizu, T. Shirasawa, M. Kajita, A. Kanayama and Y. Miyamoto, *Mech. Ageing Dev.*, 2008, **129**, (6), 322
20. D. Pedone, M. Moglianetti, E. De Luca, G. Bardi and P. P. Pompa, *Chem. Soc. Rev.*, 2017, **46**, (16), 4951

21. L. Ma, S.-J. Ding and D.-J. Yang, *Dalt. Trans.*, 2018, **47**, (47), 16969
22. D. M. D. Formaggio, X. A. de Oliveira Neto, L. D. A. Rodrigues, V. M. de Andrade, B. C. Nunes, M. Lopes-Ferreira, F. G. Ferreira, C. C. Wachesk, E. R. Camargo, K. Conceição and D. B. Tada, *J. Nanoparticle Res.*, 2019, **21**, (11), 244
23. T. Bian, H. Zhang, Y. Jiang, C. Jin, J. Wu, H. Yang and D. Yang, *Nano Lett.*, 2015, **15**, (12), 7808
24. Z. Y. Bao, D. Y. Lei, R. Jiang, X. Liu, J. Dai, J. Wang, H. L. W. Chan and Y. H. Tsang, *Nanoscale*, 2014, **6**, (15), 9063
25. C. Fang, G. Zhao, Z. Zhang, Q. Ding, N. Yu, Z. Cui and T. Bi, *Chem. Eur. J.*, 2019, **25**, (30), 7351
26. G.-H. Han, K. Y. Kim, H. Nam, H. Kim, J. Yoon, J.-H. Lee, H.-K. Kim, J.-P. Ahn, S. Y. Lee, K.-Y. Lee and T. Yu, *Catalysts*, 2020, **10**, (6), 650
27. Z. Lou, M. Fujitsuka and T. Majima, *ACS Nano*, 2016, **10**, (6), 6299
28. H. Zhang and N. Toshima, *J. Colloid Interface Sci.*, 2013, **394**, 166
29. D. Fernández-Valdés, C. Torres-Torres, C. L. Martínez-González, M. Trejo-Valdez, L. H. Hernández-Gómez and R. Torres-Martínez, *J. Nanoparticle Res.*, 2016, **18**, (7), 204
30. E. A. Hurtado-Aviles, J. A. Torres, M. Trejo-Valdez, C. R. Torres-SanMiguel, I. Villalpando and C. Torres-Torres, *Materials*, 2019, **12**, (11), 1791
31. D. Singh, A. Kumar, V. Bhalla and R. K. Thakur, *Mod. Phys. Lett. B*, 2018, **32**, (21), 1850248
32. D. Singh, S. Tripathi, D. K. Pandey, A. K. Gupta, D. K. Singh and J. Kumar, *Mod. Phys. Lett. B*, 2011, **25**, (31), 2377
33. V. Bhalla, R. Kumar, C. Tripathy and D. Singh, *Int. J. Mod. Phys. B*, 2013, **27**, (22), 1350116
34. A. Nanda, A. Tiadi, S. K. Mallik, R. Giri and G. Nath, *IOP Conf. Ser. Mater. Sci. Eng.*, 2018, **360**, 012064
35. M. Leena and S. Srinivasan, *J. Mol. Liquid.*, 2015, **206**, 103
36. M. N. Rashin and J. Hemalatha, *J. Mol. Liquid.*, 2014, **197**, 257
37. N. Yadav, A. K. Jaiswal, K. K. Dey, V. B. Yadav, G. Nath, A. K. Srivastava and R. R. Yadav, *Mater. Chem. Phys.*, 2018, **218**, 10
38. G. Vaish, R. Kripal and L. Kumar, *J. Mater. Sci.: Mater. Electron.*, 2019, **30**, (17), 16518
39. N. Yadav, P. Chaudhary, K. K. Dey, S. Yadav, B. C. Yadav and R. R. Yadav, *J. Mater. Sci.: Mater. Electron.*, 2020, **31**, (20), 17843
40. J. A. García-Merino, D. Torres-Torres, C. Carrillo-Delgado, M. Trejo-Valdez and C. Torres-Torres, *Optik*, 2019, **182**, 443
41. H. E. Toma, V. M. Zamarion, S. H. Toma and K. Araki, *J. Braz. Chem. Soc.*, 2010, **21**, (7), 1158
42. B. Karthikeyan and M. Murugavelu, *Sensors Actuators B: Chem.*, 2012, **163**, (1), 216
43. E. Grabowska, M. Marchelek, T. Klimczuk, W. Lisowski and A. Zaleska-Medynska, *J. Mol. Catal. A: Chem.*, 2016, **424**, 241
44. P. Venkatesan and J. Santhanalakshmi, *Langmuir*, 2010, **26**, (14), 12225
45. Mougin, D. Wilkinson, K. J. Roberts, R. Jack and P. Kippax, *Powder Technol.*, 2003, **134**, (3), 243
46. A. Sepehrinezhad and V. Toufigh, *Ultrasonics*, 2018, **89**, 195
47. R. R. Yadav, G. Mishra, P. K. Yadawa, S. K. Kor, A. K. Gupta, B. Raj and T. Jayakumar, *Ultrasonics*, 2008, **48**, (6–7), 591
48. A. Abu-Bakr, R. A. Pethrick and J. Emery, *Polymer*, 1982, **23**, (10), 1446
49. P. Awasthi, PhD Thesis, University of Allahabad, Old Katra, India, 2005
50. S. K. Kor, U. S. Tandon and G. Rai, *Phys. Rev. B*, 1972, **6**, (6), 2195
51. A. Józefczak and A. Skumiel, *J. Phys. Condens. Matter*, 2006, **18**, (6), 1869
52. R. J. Urick, *J. Acoust. Soc. Am.*, 1948, **20**, (3), 283
53. S. Biwa, Y. Watanabe, S. Motogi and N. Ohno, *Ultrasonics*, 2004, **43**, (1), 5
54. F. Babick, F. Hinze and S. Ripperger, *Colloids Surf. A: Physicochem. Eng. Asp.*, 2000, **172**, (1–3), 33
55. V. Pandey, G. Mishra, S. K. Verma, M. Wan and R. R. Yadav, *Mater. Sci. Appl.*, 2012, **03**, (9), 664
56. R. Prasher, P. Bhattacharya and P. E. Phelan, *Phys. Rev. Lett.*, 2005, **94**, (2), 025901
57. D. H. Kumar, H. E. Patel, V. R. R. Kumar, T. Sundararajan, T. Pradeep and S. K. Das, *Phys. Rev. Lett.*, 2004, **93**, (14), 144301
58. R. Parashar, M. Wan, R. R. Yadav, A. C. Pandey and V. Parashar, *Mater. Lett.*, 2014, **132**, 440
59. A. S. Darling, *Platinum Metals Rev.*, 1962, **6**, (3), 106

The Authors

Alok Kumar Verma is currently working as Assistant Professor in the Department of Physics, Prof. Rajendra Singh (Rajju Bhaiya) Institute of Physical Sciences for Study and Research, V.B.S. Purvanchal University, Jaunpur, India. He received his PhD degree in Physics from Department of Physics, University of Allahabad, India. His area of specialisation comprises optical, ultrasonic and thermal characterisation of nanostructured and thermoelectric materials for advanced applications. His research interests also include particles with superluminal velocity.

Navneet Yadav obtained his MSc in Physics with Spectroscopy and recently obtained PhD in Physics from the University of Allahabad, India. His research interests are in synthesis and characterisation of noble metals for antibacterial, anticancer, heat transfer and sensing applications.

Shakti Pratap Singh obtained his MSc in Physics with Spectroscopy and received his PhD degree from the Physics Department, University of Allahabad, India, in the field of Ultrasonics and Materials Science. He is currently working as Postdoctoral Fellow in the Department of Physics, Prof. Rajendra Singh (Rajju Bhaiya) Institute of Physical Sciences for Study and Research, Veer Bahadur Singh Purvanchal University, Jaunpur, India. His research interests are in the field of thermal and ultrasonic non-destructive characterisation of advanced materials for industrial applications.

Kajal Kumar Dey is currently serving as a Scientist/Assistant Professor and Head of Department at the Centre for Nanoscience and Technology of the Professor Rajendra Singh Institute of VBS Purvanchal University, Jaunpur, India. He did his doctoral research at the National Physical Laboratory (NPL), New Delhi in collaboration with the department of Physics, University of Allahabad. He worked as a SERB National Postdoctoral Fellow at the department of Chemistry of Indian Institute of Technology, Delhi. His research interests include catalysts and electrodes for water splitting reactions, the application of nanomaterials in antibacterial technology, gas sensing and coolant materials.

Devraj Singh is Professor in Department of Physics and Director of the Prof. Rajendra Singh (Rajju Bhaiya) Institute of Physical Sciences for Study and Research, Veer Bahadur Singh Purvanchal University, Jaunpur, India. He obtained his DPhil in Science at the University of Allahabad in 2002. His research and publication interests include the mechanical, thermophysical and ultrasonic characterisation of condensed and advanced materials. He is a Fellow of the Ultrasonic Society of India and a life member of a number of scientific societies. He has 91 research articles published in national and international journals of ultrasonic and materials science and 24 published books to his credit.

Professor Raja Ram Yadav is Ex-Vice-Chancellor VBS Purvanchal University and Professor of Physics at the Department of Physics, University of Allahabad. His research interests are in the non-destructive ultrasonic and thermal characterisation of nanomaterials, lyotropic liquid crystalline materials, intermetallics and semiconductors; the development of nanomaterials for biomedical applications; and theoretical calculations of nonlinear elastic and ultrasonic properties of crystalline materials. Professor Yadav successfully coupled ultrasonics with nanoscience and technology recognised as the new area of 'Ultrasonics in Nanoparticles-Liquid Suspensions' in the field of acoustics. He has 140 research articles.